Noname manuscript No.
(will be inserted by the editor)

Dynamics analysis and image encryption application of Hopfield neural network with a novel multistable and highly tunable memeristor

Wei Yao · Jiapei Liu · Yichuang Sun · Jin Zhang · Fei Yu · Li Cui · Hairong Lin

Received: 29 July 2023 / Accepted: 18 Sep 2023

Abstract Building artificial neural network (ANN) models and studying their dynamic behaviours is extremely important from both a theoretical and practical standpoint due to the rapid advancement of artificial intelligence. In addition to its engineering applications, this article concentrates primarily on the memristor model and chaotic dynamics of the asymmetric memristive neural network. First, we develop a novel memristor model, which is multistable and highly tunable . Using this memristor model to build an asymmetric memristive Hopfield neural network (AMHNN), the chaotic dynamics of the proposed AMHNN are investigated and analyzed using fundamental dynamics techniques such as equilibrium stability, bifurcation diagrams, and Lyapunov exponents. According to the findings of this study, the proposed AMHNN possesses a number of complex dynamic properties, including scaling amplitude chaos with coupling strength control, and coexisting uncommon chaotic attractors with initial control and coupling strength control. Significantly, the proposed AMHNN have been observed to exhibit the phenomenon of infinitely persisting uncommon chaotic attractors. In the interim, a system for image encryption based on the proposed AMHNN is constructed. By analyzing correlation, information entropy, and key sensitivity, the devised encryption method reveals a number of benefits. The feasibility of the encryption method is validated through field-programmable gate arrays (FPGAs) hardware experiments, and the proposed memristor and AMHNN models have been translated into a Simulink model.

Keywords Chaotic dynamics · Asymmetric memristive Hopfield neural network · Highly tunable memristor · Lyapunov exponents and bifurcation · Image encryption

W. Yao · J. Liu · J. Zhang · F. Yu
School of Computer and Communication Engineering, Changsha University of Science and Technology, Changsha 410114, China
E-mail: yaowei@csust.edu.cn
W. Yao
Key Laboratory of Computing and Stochastic Mathematics (Ministry of Education), School of Mathematics and Statistics, Hunan Normal University, Changsha, Hunan 410081, P. R. China
State Key Laboratory of Industrial Control Technology, Zhejiang University, China
Y. Sun
School of Engineering and Computer Science, University of Hertfordshire, Hatfield AL109AB
L. Cui
School of Information and Electrical Engineering, Hunan University of Science and Technology, Xiangtan 411201, China
H. Lin
College of Information Science and Engineering, Hunan University, Changsha, 410082, China

1 Introduction

Due to its nonlinearity and synaptic-like properties, memristor is a crucial new technology for memory and neuromorphic computing. The memristor was theorized in 1971 by Dr. Leon Chua[1] and was first fabricated by a research team at Hewlett-Packard Labs in 2008[2]. Since then, memristor research has exploded, as evidenced by a significant number of papers. As an important research content, mathematical memristor model is concerned and it is used to simulate the rich features of nano-memristor[3].To study the nonlinear dynamics of memristor-based circuits, to create new hybrid hardware architectures that combine memory storage and data processing at the same physical location, and to understand how biological systems work, it is very important to have such mathematical memristor model. Thankfully, many significant theories on mathematical memristor models were proposed by Chua, who categorized them as ideal memristor, generic memristor, and extended memristor. These theories provide a suitable theoretical foundation for further study on mathematical memristors. In recent times, numerous models of memristors have emerged[4, 5], in accordance with the aforementioned theory. Also, since many phenomena in reality are multistable, recently, there have been many studies on multistable memristor systems[6, 7].

Recently, with the rapid development of AI, artificial neural networks (ANNs) have gained popularity as a model in the field of machine learning and have become a strong competitor to traditional regression and statistical models in terms of practicality and effectiveness. Meanwhile, many different types of ANNs have recently emerged[8–13], and are widely used in various fields such as classification, clustering, pattern recognition and prediction, etc.

Specifically, ANN is constructed using interconnected units or nodes known as artificial neurons, which serve as a loose representation of the neurons found in a biological brain. Similar to the synapses in a biological brain, each connection within an ANN has the ability to transmit signals to other neurons. Moreover, based on the fact that memristor can simulate biological neural synapses, therefore, it can serve as synapse in artificial neural networks and artificial neuron, such as Hodgkin-Huxley neuron model, FitzHugh-Nagumo neuron model, Morris-Lecar neuron model, Hindmarsh-Rose neuron model, Chay neuron model, Hopfield neural network (HNN), Cellular neural network, etc[14–17].

Due to its distinct network topology and numerous chaotic dynamics that resemble brain function, HNN is one of these models that is frequently used as a typical paradigm[18]. Researchers have thoroughly investigated chaotic dynamics based on the HNNs for many years and from a variety of angles. For example, in recent research[6, 19], it was found that memristive HNN can well simulate the dynamic behavior of the human brain, such as periodic motion, limit cycles, chaos, coexistence chaos, etc.

Using memristors to simulate synapses in a HNN with some neurons, for instance, can result in memristive HNN with complex multistability [20–22]. Specifically, a recent study[23] demonstrated that a memristive asymmetric neural network with two sub-neural networks can generate brain-like complex chaotic initial-boosted behavior. This indicates that memristive coupled neural networks exhibit intricate dynamic behaviors closer to the brain. Meanwhile, the circuits of memristive neural networks show higher efficiency and lower power due to the use of real nano-memristor devices[24]. Thus, the construction of a brain-like dynamical system model with complex dynamic behavior plays a good role in promoting the development of brain-like computing infrastructure and also helps brain neuroscientists use the model to find the hidden meaning behind these brain-like dynamic properties.

At the same time, with the development of information technology and multimedia communication, information security is becoming more and more important in multimedia communication[25]. As an essential component of multimedia communication, it is crucial to safeguard images, as they are intimately connected to the privacy of individuals . To protect images security, various image encryption methods are designed so far[26]. Over time, researchers have utilized a variety of techniques to enhance the security of images. Because the images have different properties as compared to text, the traditional methods such as DES, AES, and IDEA are not suitable in the case of images, then many image encryption methods are utilized in the last few decades[27, 28]. Among these approaches, chaotic encryption which uses chaotic system encryption can be very suitable for generating random number sequences that are utilized as secret keys in image encryption, because its properties such as dynamic and deterministic nature, being sensitive to initial conditions, and ergodicity[29].

Numerous studies have demonstrated that image encryption methods based on HNNs with complex chaotic behaviors provide outstanding encryption performance. Using a chaotic HNN to generate a keystream, for instance, a robust hybrid image encryption method[30] was developed. Several memristive HNN-based image encryption method with multi-scroll attractors or initial-boosted behavior have recently been reported [31, 32]. These encryption method outperform earlier systems in terms of security because of their intricate dynamic features.

From the above review, it becomes clear that two issues still need further consideration:

Firstly, the existing multistable memristor models are very complex and do not provide high tunability. In reality, synapses are extremely plastic. There is no doubt, if a suitable mathematical model of the memristor with multistability and high tunability can be provided, it will have a good practical guiding significance for the construction of nano-level memristor elements.

Secondly, multiple dynamic behaviors, such as resting state, spiking firing, bursting firing, and disorder, can be exhibited by the nervous system of the brain. And numerous dynamic phenomena, including chaotic attractors, coexisting attractors, and multi-scroll attractors, have been identified and implemented in various HNNs[33–35]. However, previous studies with respect to HNNs have focused primarily on one of their dynamic characteristics, such as chaotic behavior, multi-scroll behavior, coexisting behavior, or initial-boosted behavior. The impact of the memristor on the positioning and the amplitude of the chaotic attractor of the HNN has not yet been explored in previous studies. There is no doubt that it will help people build more realistic memristive neural network.

In light of the above analysis, this paper proposes a new general memristor mathematical model that is multistable and highly tuneable. Using this paradigm, AMHNN is constructed. We alse apply the proposed AMHNN to generate an image encryption method. The primary contributions and originality of this study are enumerated as follows:

1. We construct a novel multistable and highly tunable memristor (MSAHTM) model.
2. The AMHNN exhibits rich and complex brain-like initial-boosted dynamics, in which an infinite number of coexisting chaotic attractors with distinct shapes and positions are generated, the range and position of chaotic attractor of the AMHNN are affected by the interference coefficient. To the best of our knowledge, this peculiar feature has rarely been detected in other neural networks.
3. To demonstrate the usefulness of the proposed AMHNN , we develop an image encryption cryptosystem based on AMHNN. The developed cryptosystem offers numerous advantages over currently used chaos-based image encryption methods, including a wide key-space, high information entropy, extremely sensitive keys, and good robustness.
4. Hardware experiments using FPGAs are carried out to show the effctiveness of the image cryptosystem.

The rest of this paper is organized as follows: Section 2 derives the novel generic multistable memristor model from the circuit perspective and builds its Simulink model. Section 3 designs the AMHNN, constructs their Simulink models, and analyzes their dynamic performance. Section 4 designs an image encryption method based on AMHNN, discusses its performance, and verifies it on the FPGA hardware platform. Section 5 summarizes and discusses the whole work.

2 CONSTRUCTION OF THE NOVEL MEMRISTOR MODEL

A voltage-controlled generic memristor can be described as follows in accordance with memristor theory[36]:

State equation:

$$dx/dt = g(x, v), \tag{1}$$

State-dependent Ohm's law:

$$i = G(x)v, \tag{2}$$

where $G(x)$ is memductance, and v, i, and x denote voltage, current, and memristor state, respectively. Now, based on equations (1) and (2), we propose the MSAHTM:

$$dx/dt = g(x, v) = acos(x)tanh(x) - v, \tag{3}$$

$$i = G(x)v = (bx + ccos(x))v. \tag{4}$$

In this work, a, b, and c are set to 3, 500 and 0.4, respectively.

To better study this new model, a sinusoidal external stimulus is applied to the memristor:

$$v = Asin(Ft). \tag{5}$$

where A and F respectively represent amplitude and frequency. And a more in-depth characteristic analysis is provided in the next section using numerical simulations by MATLAB.

2.1 Volt-ampere characteristic analysis

Equations (3) and (4) are examined when the stimulus $v = Asin(Ft)$ is used as the driving source at various frequencies and amplitudes. The pinched hysteresis loops of the memristor are numerically simulated and depicted in Fig. 1, where initial state $x(0) = \frac{\pi}{2}$, amplitudes A and frequencies F are chosen with various values. Three pinched hysteresis loops running through the origin in the voltage-current (v-i) plane are clearly visible in Fig. 1(a). And in Fig. 1(b), the hysteresis lobe area steadily decreases as the excitation frequency rises from 0.8 to 8. Furthermore, it is obvious that the pinched hysteresis loop will trend to a single-valued curve as the frequency approaches infinity.The novel model is thus a memristor device, since it has three memristor fingerprints[37].

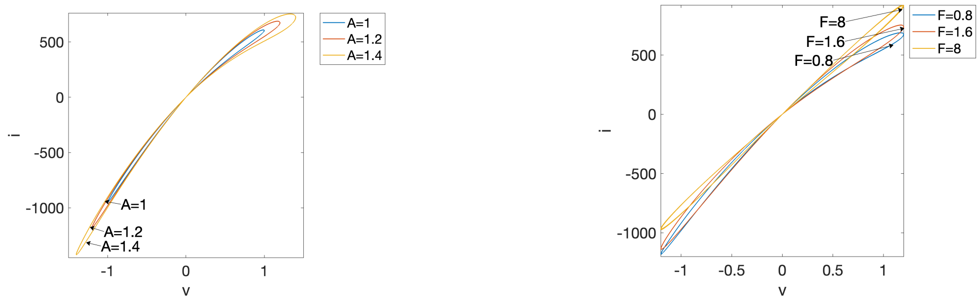

(a) (b)

Fig. 1 Pinched hysteresis loops of MSAHTM under $v = Asin(Ft)$ with initial state $x(0)=\frac{\pi}{2}$. (a) Three pinched hysteresis loops running through the origin with different amplitudes. (b) The hysteresis lobe area steadily decreasing as the excitation frequency rises from 0.8 to 8.

2.2 Multistability analysis

Here, we show the multistability of MSAHTM using a power-off plot (POP). Typically, POP is just a curve in the $f(x, 0)$ vs x plane [38]. Due to the fact that $dx/dt = 0$, any intersection of POP with the x-axis is defined as an equilibrium point of the memristor. Then, assuming $v = 0$, the memristor state (3) becomes:

$$dx/dt = g(x, 0) = acos(x)tanh(x), \tag{6}$$

where a satisifies the equation (3).

The POP of this innovative memristor is seen in Fig. 2. In Fig. 2, there exist an unlimited number of intersections, which correspond to equilibrium points. As shown by the evaluation tool in [38], the equilibrium points with circle dots are asymptotically stable, while the equilibrium points with triangle dots are unstable. Evidently, given random initial states, the memristor state tends toward the equilibrium point x_e:

$$x_e = \pm\frac{(2k+1)\pi}{2}, k \in (0, 1, 2, 3, 4 \ldots), \tag{7}$$

In particular, the stable equilibrium point x_{se} can be expressed as follows:

$$x_{se} = \pm\frac{(4k+1)\pi}{2}, k \in (0, 1, 2, 3, 4 \ldots). \tag{8}$$

Fig. 2 shows that MSAHTM makes six coexisting pinched hysteresis loops on the v-i plane. It could produce an infinite number of coexisting pinched hysteresis loops for different initial states. This also indicates that MSAHTM is also locally active for the branches of the state $x(0) < 0$, as indicated by the fact that its slope at origin is negative.

2.3 Tunability analysis

More interestingly, as we can see from Fig. 3, this memristor model can generate different shapes of hysteresis loops, with varying a, b, and c parameters. By setting b = 5, c = 0.4, and altering a from -2 to 3, for instance, this model can generate various shapes of hysteresis loops. And by setting a = 3, c = 0.4, and varying b between -50 and 50, hysteresis loops approximately spins in counterclockwise. Hysteresis loops pull up to the upper left when a = 3, b = 5, and c varies from -4 to 6. As a result of the analysis, it is clear that this MSAHTM is highly tunable, thus simulating the dynamic behavior of various types of memristor devices.

2.4 Simulink model of novel memristor

In order to further verify this novel memristor, we developed the Simulink model of it, which can be seen from its circuit diagram in Fig. 4(a). Furthermore, the simulation results of this Simulink model are shown in Fig. 4(b).

3 APPLICATION IN A HOPFIELD NEURAL NETWORK

3.1 Construction of memristive Hopfield neural network

A HNN is often used to mimic the dynamic activity of brain processes[6], for better understanding human memory. The i-th neuron in HNN can be stated as

$$C_i\dot{x}_i = -x_i/R_i + \sum_{j=1}^{n} w_{ij}\tanh(x_j) + I_i(i, j \in N^*). \tag{9}$$

where C_i, R_i, and x_i are, respectively, the membrane capacitance, membrane resistance, and membrane voltage between the exterior and interior of neuron i. $\tanh(x_i)$

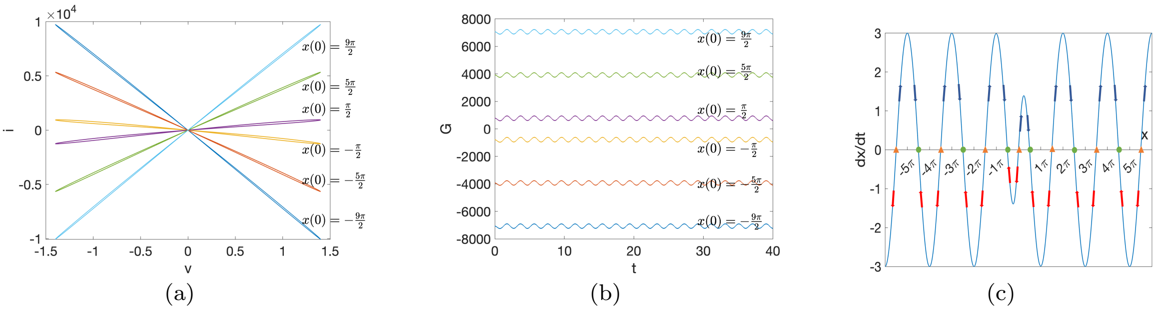

Fig. 2 (a-b) Numerical simulation results of MSAHTM under different initial states $x(0)$= -$\frac{9\pi}{2}$, -$\frac{5\pi}{2}$, -$\frac{\pi}{2}$, $\frac{\pi}{2}$, $\frac{5\pi}{2}$, $\frac{9\pi}{2}$. (c) POP of the MSAHTM.

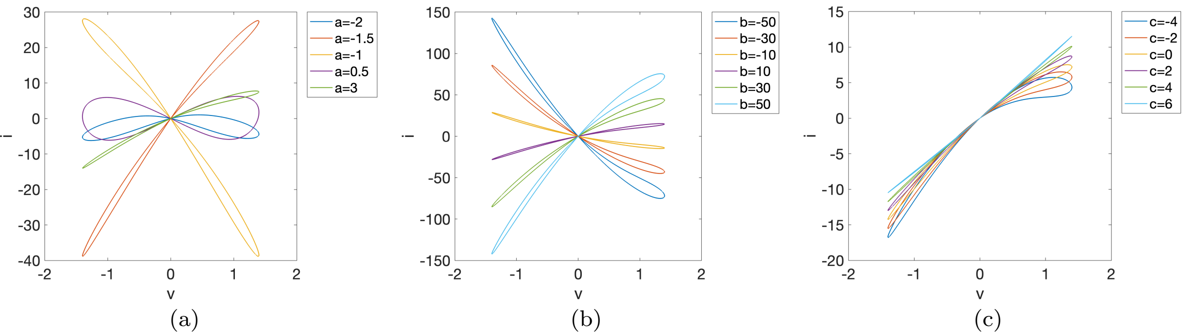

Fig. 3 Different shapes of coexisting hysteresis loops, with fixed initial state, but different parameter for memristor . (a) By setting b = 5, c = 0.4, and altering a from -2 to 3, for instance, this model can generate various shapes of hysteresis loops. (b) By setting a = 3, c = 0.4, and varying b between -50 and 50, hysteresis loops approximately spins in counterclockwise. (c) Hysteresis loops pull up to the upper left when a = 3, b = 5, and c varies from -4 to 6.

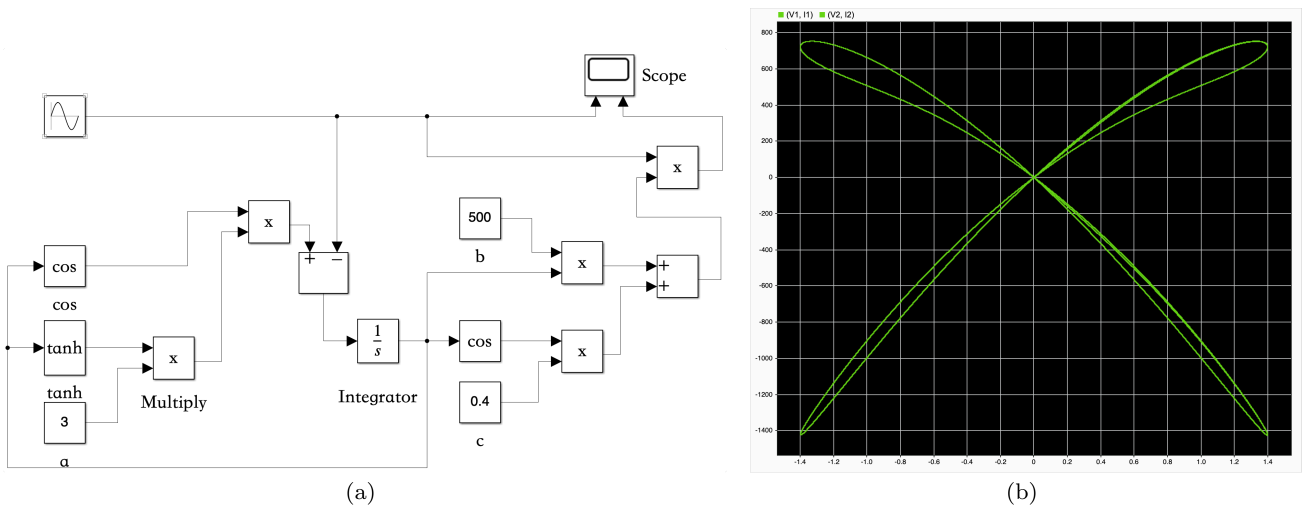

Fig. 4 Simulink model of MSAHTM. (a) Circuit diagram of MSAHTM. (b) Circuit simulation results of MSAHTM under different initial condition $x(0)$ = -$\frac{\pi}{2}$ and $x(0)$ = $\frac{\pi}{2}$.

is the activation function of the neuron, and I_i is the external bias current. From an ANN model standpoint, w_{ij} is the synaptic weight that describes the strength of the connection between neurons j and i. From an circuital standpoint, w_{ij} is the admittance of the resistor linking neuron j and neuron i. According to the characteristics of memristors, both memductance and w_{ij} are measured in Siemens, hence a memristor may be used in lieu of a connecting resistor. Thus, the synaptic weight may be converted into the memductance of a memristor. Under this strategy, some memristor-based HNNs were presented, and complex dynamic behaviors of quasi-periodic orbits, chaos and coexisting chaos were identified [39–42].

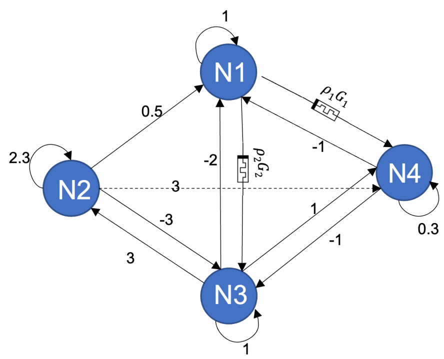

Fig. 5 Connection topologies of the AMHNN.

To better understand how this novel memristor can apply itself in HNN, we constructed a asymmetric memristive HNN, named AMHNN, which is composed of four neurons coupled with two memristors, as can be seen in Fig. 5. In this HNN model, the proposed novel memristor stands for the synaptic weights w_{41} and w_{31}. By combining equations (3), (4), and (9), assuming C_i = 1, R_i = 1, and I_i = 0, the dynamical equation of the AMHNN in Fig. 5 is as follows:

$$\begin{cases} \dot{x}_1 = -x_1 + \tanh(x_1) + 0.5\tanh(x_2) - 2\tanh(x_3) - \tanh(x_4), \\ \dot{x}_2 = -x_2 + 2.3\tanh(x_2) + 3\tanh(x_3), \\ \dot{x}_3 = -0.7x_3 + \rho_2 G_2 \tanh(x_1) - 3\tanh(x_2) + \tanh(x_3) - \tanh(x_4), \\ \dot{x}_4 = -x_4 + \rho_1 G_1 \tanh(x_1) + 3\tanh(x_2) + \tanh(x_3) + 0.3\tanh(x_4), \\ \dot{z}_1 = 3\cos(z_1)\tanh(z_1) - \tanh(x_1), \\ \dot{z}_2 = 3\cos(z_2)\tanh(z_2) - \tanh(x_1). \end{cases} \tag{10}$$

where $G_1 = 500z_1 + 0.4\cos(z_1)$, $G_2 = 500z_2 + 0.4\cos(z_2)$ indicate the synaptic weights w_{41} between neuron 1 and neuron 4, and w_{31} between neuron 1 and neuron 3, respectively. The coupling strength of the memristor is represented by the system parameters ρ_1 and ρ_2. By setting the right side of the equation (10) to zero, we can determine that the AMHNN has indefinitely discrete equilibria

$$E = \left\{ (x_1^*, x_2^*, x_3^*, x_4^*, z_1^*, z_2^*) \mid x_i^* = 0, z_1^* = \frac{(2k+1)\pi}{2}, z_2^* = \frac{(2k+1)\pi}{2} \right\} \tag{11}$$

where $i = 1, 2, 3, 4$, $k \in (0, 1, 2, 3, \ldots)$. By modifying phase space, AMHNN can create infinitely many equilibria along the z_1-axis and z_2-axis. Evidently, using two unique memristors as synapses is crucial to the formation of endless equilibria.

3.2 Dynamic analysis of AMHNN

The complex dynamic behavior in the AMHNN(10) is revealed by using basic dynamic analysis methods, including bifurcation diagrams, Lyapunov exponents, and phase diagram for further investigation. In addition, all numerical simulations are carried out in MATLAB R2021a using the Runge-Kutta algorithm(ODE45).

3.2.1 Coupling strength-relied dynamic behaviors

To explore the effect of a single coupling coefficient perturbation on the dynamic behavior of AMHNN, we assume that the initial conditions are $(x_1(0), x_2(0), x_3(0), x_4(0), z_1(0), z_2(0)) = (1, 1, 1, 1, \frac{\pi}{2}, \frac{\pi}{2})$ and we use fixed $\rho_2 = 0.008$. As shown in Fig. 6, it is obvious that AMHNN produces successively periodic attractors with varied periods and chaotic attractors as ρ_1 increases. Under prior initial conditions, the phase portraits depicting the attractors of AMHNN with various ρ_1 values are provided to highlight its dynamic evolution with the coupling strength of the memristor. In Fig. 7, by varying ρ_1, it shows that AMHNN can produce a series of chaos with different amplitude, which means the change of ρ_1 can control the amplitude of the chaotic attractors. This specific phenomena is capable of simulating brain impulses with various amplitudes that correspond to various dynamic states.

Then, to investigate whether AMHNN can achieve complex bifurcation under the perturbation of a single coupling coefficient, the bifurcation diagram of AMHNN with respect to the parameter $\rho_1 \in (-5, 5)$ can be shown in Fig. 8 (a-b). When $\rho_1 < 0$, as ρ_1 increases, x_{1max} route is a horizontal line without bifurcation and x_{4max} is a upward sloping line without bifurcation, denoting the stable equilibrium point of x_4 that receives the effect of ρ_1 and the larger ρ_1 is, the closer the stable equilibrium point of x_4 is to the coordinate origin. However, when $\rho_1 > 0$, as ρ_1 increases x_{1max} route quickly become dense bunch of points, and x_{4max} route steadily expands with dense bunch of points, indicating that the proposed AMHNN can rapidly enters chaotic states and possesses extraordinarily complex chaotic behavior.

Meanwhile, as shown in Fig. 8 (c-d), the associated constant Lyapunov exponents have one positive value

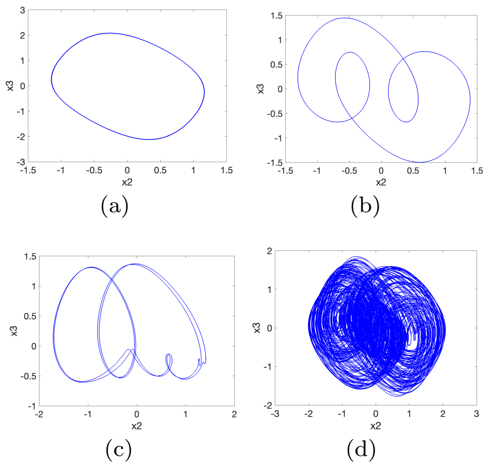

Fig. 6 Numerically simulated phase portraits for different ρ_1 with fixed ρ_2. (a) Period-1 attractor at $\rho_1 = 0.003$. (b) Period-3 attractor at $\rho_1 = 0.007$. (c) Multi-period attractor at $\rho_1 = 0.015$. (d) Chaotic attractor at $\rho_1 = 0.023$.

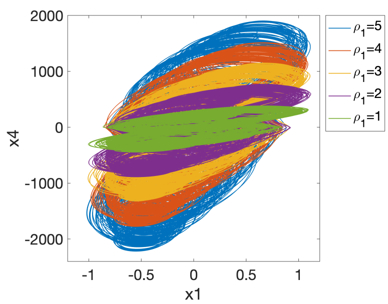

Fig. 7 A series of scaling amplitude chaos with varying ρ_1, where $\rho_1 \in (1, 5)$.

and the sum of the exponents is negative across the entire ρ_1 fluctuation range, indicating that AMHNN has a high chaotic quality. Moreover, based on the fact that AMHNN has two coupling coefficients ρ_1 and ρ_2, how the two coefficients affect the dynamic behavior of it is thoroughly investigated in Fig. 9 by variables method. In Fig. 9(a), ρ_2 is fixed with 0.008 and ρ_1 varies from 0.003 to 2.6. When $\rho_1 = 0.018$, AMHNN has entered chaotic state. While in Fig. 9(b), by contrast, ρ_1 is fixed at 0.016, we vary ρ_2 from 0.001 to 0.064. It is clear that AMHNN can generate a more complex dynamic behavior than the previous condition as ρ_2 changes. In summary, all the facts prove that the dynamic behavior of the system is highly dependent on the strength of its coupling coefficient ρ_1 and ρ_2.

3.2.2 Initial state-relied dynamic behaviors

Through the above numerical and theoretical analysis, we can make the following hypothesis: with a given coupling strength, AMHNN may generate coexisting attractors under varied initial conditions of the two memristor G_1 and G_2. In order to verify this hypothesis, several suitable simulation experiments were conducted. At first, by influencing the state evolution of G_1, how the different initial states of G_1 would affect the dynamic behavior of AMHNN is studied in this paper. After that we study the initial states of G_2. Supposing that $\rho_1 = 2.6$ and $\rho_2 = 0.008$, coexisting attractors may be seen from the initial states listed below: $(x_1(0), x_2(0), x_3(0), x_4(0), z_1(0), z_2(0)) = (1, 1, 1, 1, \frac{(4k+1)\pi}{2}, \frac{(4k+1)\pi}{2})$, where $k \in (0, 1, 2, 3, \ldots)$. Then, by choosing three different initial states with fixed $z_2(0) = \frac{\pi}{2}$, such as $(1, 1, 1, 1, \frac{\pi}{2}, \frac{\pi}{2})$, $(1, 1, 1, 1, \frac{5\pi}{2}, \frac{\pi}{2})$, $(1, 1, 1, 1, \frac{9\pi}{2}, \frac{\pi}{2})$, the AMHNN generates three coexisting chaotic attractors with different position, as demonstrated in Fig. 10 (a-b). However, when we do not fix $z_2(0)$ and choose different values for it, such as $(1, 1, 1, 1, \frac{\pi}{2}, \frac{\pi}{2})$, $(1, 1, 1, 1, \frac{5\pi}{2}, \frac{5\pi}{2})$, $(1, 1, 1, 1, \frac{9\pi}{2}, \frac{9\pi}{2})$, the AMHNN produces three coexisting attractors of different position and shapes, as demonstrated in Fig. 10 (c-d). So, for AMHNN, we can say that $z_1(0)$ governs the position of the attractors and $z_2(0)$ can change the shape of the attractors. Furthermore, Fig. 11 (a-b), show that different $z_1(0)$ can generate state evolution with different position, which means G_1 is actually a multistable memristor. While, in Fig. 11 (c-d), distinct $z_2(0)$ can cause state evolution with varying amplitudes, which can affect the dynamic behavior of the AMHNN.

3.3 Simulink model of AMHNN

To further confirm the observed attractors, we design the Simulink model of the AMHNN, and its circuit diagram can be seen in Fig. 12(a-b). Chaotic attractors can be successfully generated by Simulink model of AMHNN, which is same to numerical simulation in Fig. 9(a).

4 APPLICATION IN IMAGE ENCRYPTION

Recent emphasis has been placed on chaos-based image encryption research [43–47]. Systems with multistability are better candidates for chaos applications than chaotic systems without multistability because they have more complex dynamic behavior. Because it has both chaotic attractors and multistability, the proposed AMHNN has a lot of potential use in image encryption method. In this section, an image encryption method based on AMHNN is developed and its suitability for image secure communication is evaluated. In order to have an intuitive understanding, the architecture of the AMHNN-based image encryption method as can be shown in Fig. 13.

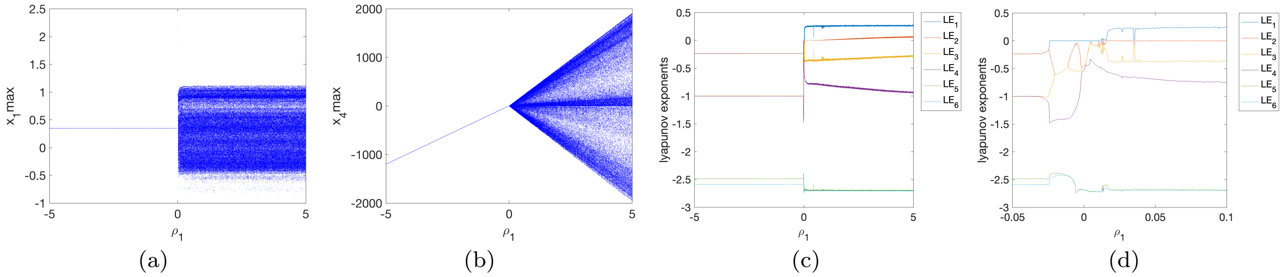

Fig. 8 (a-b) Bifurcation diagram of the x_1 and x_4 of AMHNN with $\rho_1 \in (-5, 5)$, $\rho_2 = 0.008$. (c) Six Lyapunov exponents diagram of the AMHNN, where $\rho_1 \in (-5, 5)$. (d) Six Lyapunov exponents diagram of the AMHNN, where $\rho_1 \in (-0.05, 0.1)$.

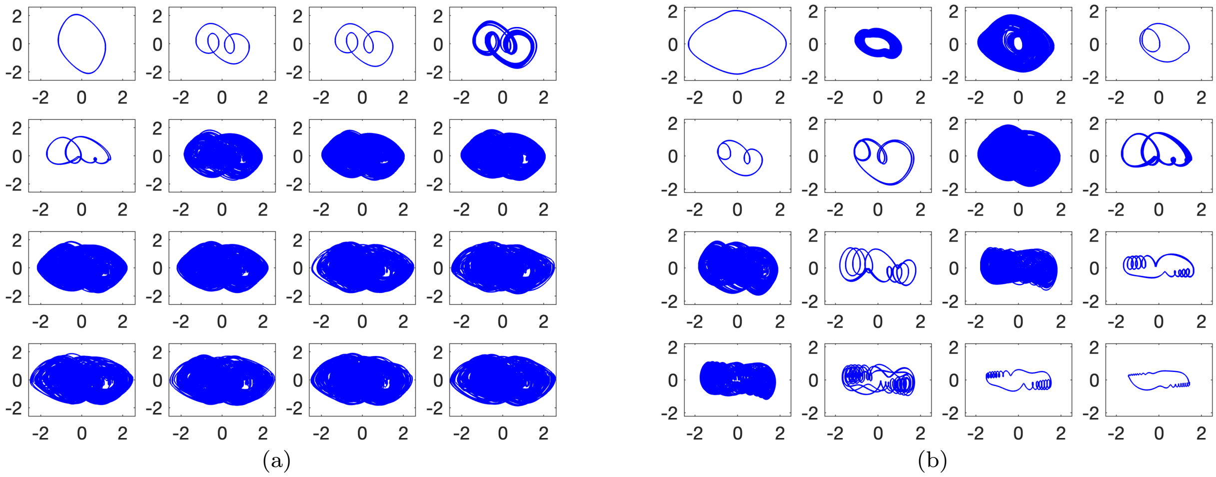

Fig. 9 An abundance of dynamic behavior with various coupling strength and $(x_1(0), x_2(0), x_3(0), x_4(0), z_1(0), z_2(0)) = (1,1,1,1,\frac{\pi}{2},\frac{\pi}{2})$, where the x-axis represents x_2 and the y-axis represents x_3. (a)In this case, ρ_2 equals 0.008, ρ_1 ranges from 0.003 to 2.6. The specific values of parameter ρ_1, by row traversal order, are [0.0030 0.0060 0.0090 0.0120 0.0150 0.0180 0.0210 0.0240 0.0360 0.0390 0.1260 0.1590 1.6000 1.6300 1.6500 2.6000]. (b) In this case, ρ_1 equals 0.016, ρ_2 ranges from 0.001 to 0.064. The specific values of parameter ρ_2, by row traversal order, are [0.0010 0.0020 0.0030 0.0040 0.0050 0.0060 0.0070 0.0080 0.0110 0.0190 0.0210 0.0220 0.0240 0.0280 0.0440 0.064].

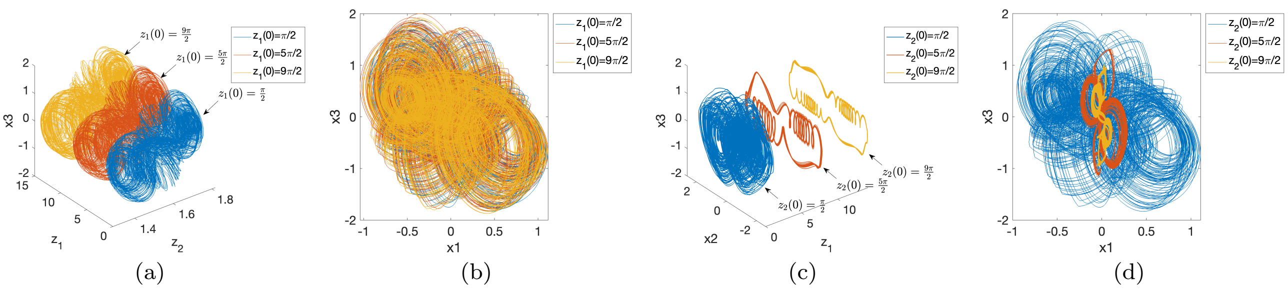

Fig. 10 (a-b) Three coexisting chaotic attractors of different positions on phase space with different initial conditions $z_1(0)$, where $\rho_1 = 2.6$, $\rho_2 = 0.008$ and $z_2(0) = \frac{\pi}{2}$. (c-d) Coexisting uncommon attractors with different shapes on phase space with different initial conditions $z_2(0)$, where $\rho_1 = 2.6$, $\rho_2 = 0.008$ and $z_1(0)$ is equal to $z_2(0)$.

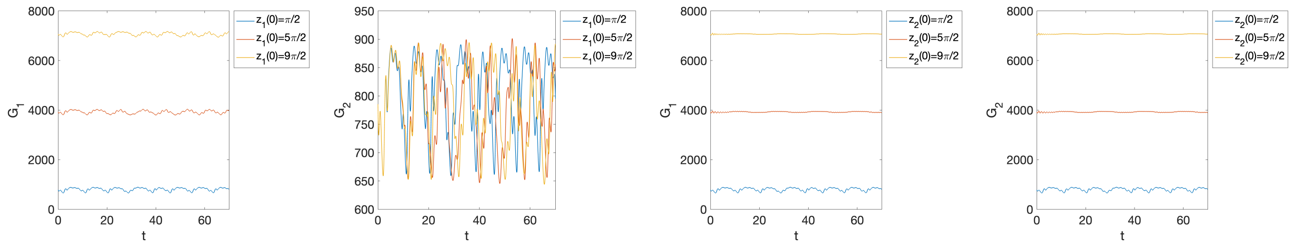

(a) (b) (c) (d)

Fig. 11 (a-b) The state evolution of G_1 and G_2 with different $z_1(0)$, where $\rho_1 = 2.6$, $\rho_2 = 0.008$ and $z_2(0) = \frac{\pi}{2}$. (c-d) The state evolution of G_1 and G_2 with different $z_2(0)$, where $\rho_1 = 2.6$, $\rho_2 = 0.008$ and $z_1(0)$ is equal to $z_2(0)$.

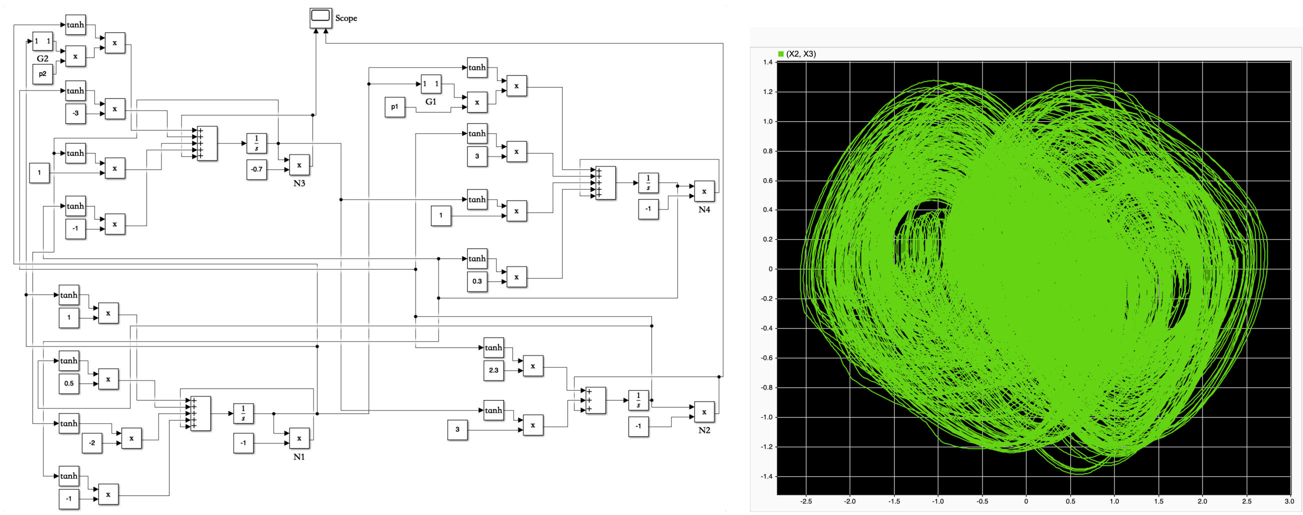

(a) (b)

Fig. 12 Simulink model of the AMHNN. (a) Circuit diagram of the AMHNN. (b) Chaotic attractors obtained from the AMHNN circuit in simulink simulation, where $(x_1(0), x_2(0), x_3(0), x_4(0), z_1(0), z_2(0)) = (1,1,1,1,\frac{\pi}{2},\frac{\pi}{2})$, $\rho_1 = 2.6$, and $\rho_2 = 0.008$.

4.1 Description of encryption method

1. Image serialization and deserialization module: Select the original image ORI, suppose the size of the image is (A × B), and serialize the 2D image by column-first scanning to obtain the 1D image sequence $O(i)$, the sequence length is (A × B). After encryption, arrange the encrypted sequence $E'(i)$ in columns to form an encrypted image ENC of size (A × B).
2. Chaotic sequence generator: Set system settings, control parameters, initial states, the discarded number N_0, and time step T, then iterate the AMHNN using the Runge-Kutta algorithm(ODE45). Six discrete chaotic sequences of the same length are created here: $(x_1(i), x_2(i), x_3(i), x_4(i), z_1(i), z_2(i))$.
3. Key generator: Following is how the chaotic sequences are reprocessed:

$$\begin{cases} A(i) = ((x_1(i) + x_2(i) + x_3(i) + x_4(i) + z_1(i) + z_2(i))/6) * 10^{13}, \\ K(i) = mod(floor(A(i)), 256). \end{cases} \tag{12}$$

Here, $A(i)$ is chaotic sequence generated by AMNN and $K(i)$ is generated by modulo operation on $A(i)$, where $floor(x)$ represents the largest integer less than or equal to x.

4. Permutation and Diffusion module: Here, we use the arnold cat map (ACM) to jumble the original image, since it may considerably minimize the connection between image pixels[48, 49]. Consequently, obtaining this design may improve the encryption process.

$$\begin{cases} Ki = K(i)\,[randi(floor(len(K(i)) * 0.8), len(K(i)))], \\ Li = K(i)\,[randi(floor(len(K(i)) * 0.5), floor(len(K(i)) * 0.7))]. \end{cases} \tag{13}$$

$$\begin{bmatrix} I' \\ J' \end{bmatrix} = \begin{bmatrix} 1 & K_i \\ L_i & K_i L_i + 1 \end{bmatrix} \begin{bmatrix} I \\ J \end{bmatrix} mod\ N. \tag{14}$$

$$E^{'}(i) = P(i) \oplus K(i). \tag{15}$$

where the symbol $\oplus$ represents the XOR operation.

In this case, $K(i)$[x] means selecting value from $K(i)$ by x-th position, $randi(x, y)$ represents returning a random integer from $[x, y]$, and $len(K(i))$ returns the length of the $K(i)$ sequence. K_i and L_i are the system parameters of ACM, I and J represent the

original pixel position, I' and J' represent the pixel position after scrambling, and N is equal to the small one between A and B. Traverse and scramble all the elements in the image sequence $O(i)$, perform ACM $abs(K_i - L_i)/2$ times until the scrambling is completed, and obtain the scrambling sequence $P(i)$. Then, perform a bitwise XOR operation(15) on $P(i)$ and $K(i)$ to realize the diffusion of the image encryption process and obtain the encrypted sequence $E^{'}(i)$.
5. Decryption module: The encrypted image is decrypted with the reverse process of the encryption method.

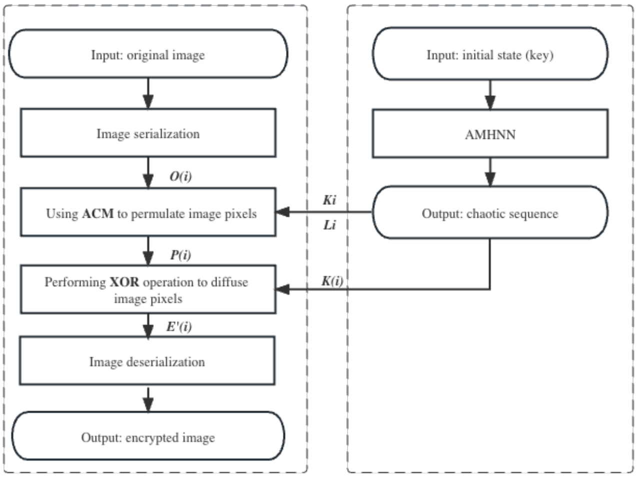

Fig. 13 Architecture of the AMHNN-based image encryption method.

4.2 Experiments and Performance Analyses

1. Key space analysis:
   The secret key of the proposed scheme consists of eight parameters $(x_1(0), x_2(0), x_3(0), x_4(0), z_1(0), z_2(0), \rho_1, \rho_2)$, where $x_1(0), x_2(0), x_3(0), x_4(0), z_1(0), z_2(0), \rho_1, \rho_2$ are double numbers. Then the key space of the proposed scheme is $(10^{16})^8 = 10^{128} \approx 2^{384}$ with the accuracy of 10^{-14}. Therefore, our scheme can resist the brute-force attack.
2. Differential attack analysis:
   In this attack, the hacker slightly alters the plaintext or original image to get around the encryption method. The Unified Averaged Change Intensity (UACI) and Number of Pixel Change Rate (NPCR) are two measures that are used to assess how vulnerable a certain encryption method is to a differential attack. The difference between the original plaintext and the encrypted ciphertext is compared to calculate the average level of intensity. Two cipher images C_1 and C_2, which differ by only one pixel and whose sizes are equal to $M \times N$. The expressions $C_1(i,j)$ and $C_2(i,j)$, respectively, represent the gray values of the pixels at positions (i,j) of C_1 and C_2. NPCR and UACI can be written as:

$$\mathrm{NPCR}(C_1, C_2) = \sum_{i=1}^{M} \sum_{j=1}^{N} \frac{D(i,j)}{MN} \times 100\% \tag{16}$$

$$D(i,j) = \begin{cases} 0, & if C_1(i,j) = C_2(i,j) \\ 1, & if C_1(i,j) \neq C_2(i,j) \end{cases} \tag{17}$$

$$\mathrm{UACI}(C_1, C_2) = \frac{1}{MN} \sum_{i=1}^{M} \sum_{j=1}^{N} \frac{|C_1(i,j) - C_2(i,j)|}{255} \times 100\%. \tag{18}$$

The expected NPCR and UACI values of a grayscale image are 99.6094% and 33.4635%, respectively, according to [50,18]. The NPCR and UACI values of the encrypted images for various plain images using the suggested encryption method are provided in Table 1.The numbers for NPCR and UACI for the provided encryption method in Table 1 are quite similar to those expected values. As a result, it is extremely sensitive to even minor changes in the basic images. That is to say, it has a potent defense against differential attacks.

Table 1 Results of UACI and NPCR test for experimental datasets

Image	NPCR(%)	UACI(%)
Airplane	98.8638	31.3101
Monkey	96.6558	33.0489
Dog	99.3958	32.8813

3. Histogram analysis:
   The histogram of an image depicts the intensity distribution of the image pixels. Generally speaking, a decent encryption method can provide an image with a uniform histogram that is resistant to statistical assault[51]. Fig. 14(a-f), depict the original images and histograms. Fig. 14(g-l) exhibit, respectively, the encrypted images and accompanying histograms. As shown, the histograms of the encrypted images are very uniform and notably different from the histograms of the original images, indicating that the encryption method based on the proposed AMHNN can withstand statistical assault well.
4. Correlation analysis:
   The pixels near one another in the horizontal, vertical, and diagonal directions of the original image exhibit a high association. In contrast, the correlation coefficients in an encrypted image should be near zero in three dimensions. The correlation[52] of each pair of pixels could be calculated by

$$\rho_{xy} = \frac{\sum_{i=1}^{N}(x_i - E(x))(y_i - E(y))}{\sqrt{\sum_{i=1}^{N}(x_i - E(x))^2}\sqrt{\sum_{i=1}^{N}(y_i - E(y))^2}}. \tag{19}$$

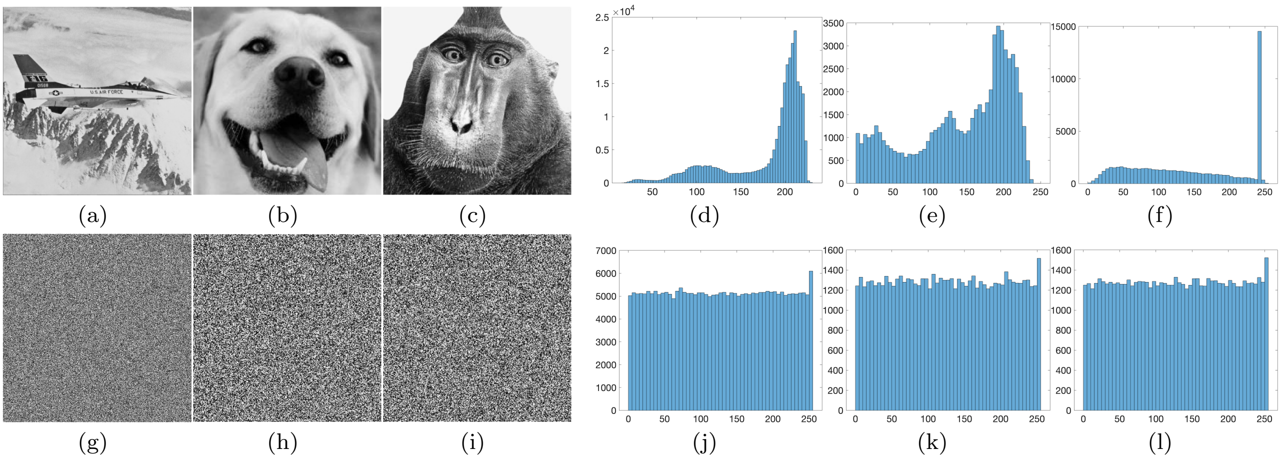

Fig. 14 Experiment results of the proposed encryption method. (a-c) Original image. (d-f) Histogram of the original image. (g-i) Encrypted image. (j-l) Histogram of the encrypted image.

N is the total number of pixels, and $E(x)$ and $E(y)$ are the mean values of x and y, respectively. Here, we compare the correlation distribution between neighboring pixels of the encrypted image and the original image in three orientations.
After encryption, it is evident from Fig. 15 and Table 2 that the correlation distribution of the encrypted image gets jumbled, and its correlation coefficients trend toward 0.

5. Entropy analysis:
When assessing the unpredictability of an encrypted image, the information entropy is a crucial metric. If an encryption method is capable of producing encrypted images with a maximum information entropy close to 8, it has great randomness properties[53]. In experiments, we may use the following formula(20) to determine the information entropy:

$$H(m) = -\sum_{i=1}^{L} P(m_i) \log_2^{P(m_i)} . \tag{20}$$

Here, the entropies of the original image, the encrypted image, and the decrypted image are calculated using the equation (20). Additionally, the entropies of these images, which can be found in Table 2, demonstrate that the encrypted images created by this encryption method are extremely close to 8, indicating that this encryption method can provide good security in the domain of image encryption.

6. Key sensitivity analysis:
Key sensitivity is a critical index for the security of encryption methods. A successful encryption method should be sensitive to the key. In our encryption technique, both the system parameter and the initial state ($x_1(0)$, $x_2(0)$, $x_3(0)$, $x_4(0)$, $z_1(0)$, $z_2(0)$, ρ_1, ρ_2) serve as secret keys. The correctly decrypted image is shown in Fig. 16 (a,e,i). And the others depicts the erroneous decrypted images resulting from a little modification of the secret keys. It can be seen that even the secret key has been changed a bit, by adding 10^{-14}, the decrypted image is completely different from the original image. Therefore, the key sensitivity test proves that the proposed image encryption method has complete sensitivity to the key.

In this study, we conducted a comparison between the results of the presented cryptosystem and those of previous similar works, as shown in Table 3. It is evident that the chaotic system utilized in the designed encryption method possesses higher dimensions and more complex chaotic dynamics when compared to the recent results of [54], [55], and [18]. As a result, the proposed image encryption method offers a higher information entropy, and a more sensitive secret key, thereby ensure enhanced security. Additionally, the designed image encryption method demonstrates very low correlation coefficients in all directions. Consequently, these findings suggest that the image encryption method based on the AMHNN can effectively withstand entropy attacks and statistical attacks, making it suitable for safeguarding image data in practical information communication scenarios.

4.3 Implementation of encryption method in FPGA

The FPGA is widely used in industrial electronics due to its qualities of ultralow power, programmable reusability, and high controllable. In particular, FPGA-based chaotic systems have received a lot of attention recently [18, 55]. However, FPGA hardware is seldom used to create image cryptosystems based on chaotic neural networks [56–58]. So, in order to implement the suggested AMHNN and the created image encryption

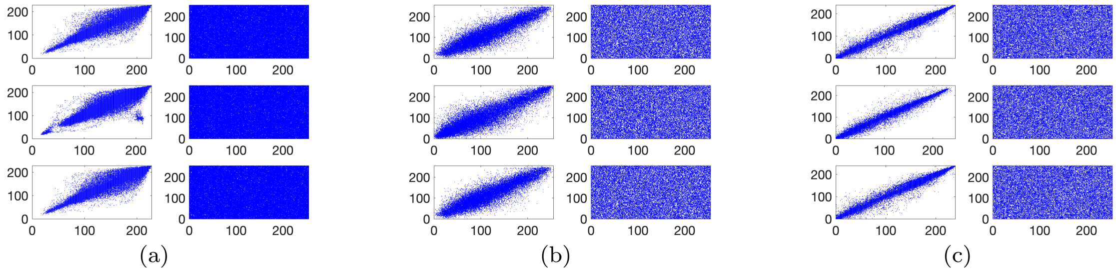

Fig. 15 The correlation distribution diagram of adjacent pixels comparison between original image and encrypted image from three directions. (a-c) The correlation distribution of airplane, monkey, dog.

Table 2 Coefficients of correlation and information entropy of the original images and their encrypted images

Image	Type	Horizontal	Vertical	Diagonal	Entropy
Airplane	Original	0.96632	0.96413	0.93702	6.7024
Airplane	Encrypted	0.00178	0.00130	0.00011	7.9992
Monkey	Original	0.95554	0.95765	0.93238	6.8841
Monkey	Encrypted	-0.00246	0.00244	-0.00480	7.9976
Dog	Original	0.98759	0.99194	0.98192	7.6806
Dog	Encrypted	0.00228	-0.00516	-0.00710	7.9977

Table 3 Performance comparison with some exsiting system

Ref	Image type	Information Entropy	Key sensitivity	Correlation: Horizontal, Vertical, Diagonal	Hardware demonstration
2020 [54]	Lena	7.9975	–	-0.0327, -0.0414, -0.0037	No
2021 [55]	Lena	7.9976	10^{-9}	0.000827, 0.005238, 0.000455	Yes
2022 [18]	Medical Image Chest	7.9981	10^{-12}	-0.001745, -0.000839, 0.013351	Yes
This work	Airplane	7.9992	10^{-14}	0.00178, 0.00130, 0.00011	Yes

method, we develop an FPGA-based hardware test platform. One Xilinx Virtex-6 FPGA development board and one monitor are part of the hardware.

The encryption and decryption functions are implemented using Verilog HDL programming, and the creation of the chaotic sequences is based on AMHNN. In the experiment, the RAM of the ZYNQ-XC7Z020 chip is used to store images. Fig. 17 displays both the original image and the encrypted image using the secret key ($x_1(0)$, $x_2(0)$, $x_3(0)$, $x_4(0)$, $z_1(0)$, $z_2(0)$, ρ_1, ρ_2) = (1, 1, 1, 1, $\frac{\pi}{2}$, $\frac{\pi}{2}$, 2.6, 0.008). The FPGA-based experimentation findings and the MATLAB-based simulation results are in complete agreement. It is clear from these experimental findings that the proposed AMHNN-based image encryption method is both feasible and trustworthy.

5 Conclusion

In this paper, we devolop a novel memristor model called MSAHTM. Then, we use MSAHTM to construct AMHNN. The proposed AMHNN exhibits rich and complex brain-like initial-boosted dynamics, where infinitely many coexisting chaotic attractors sharing the same shape but with different position are generated. To the best of our knowledge, this peculiar feature has rarely

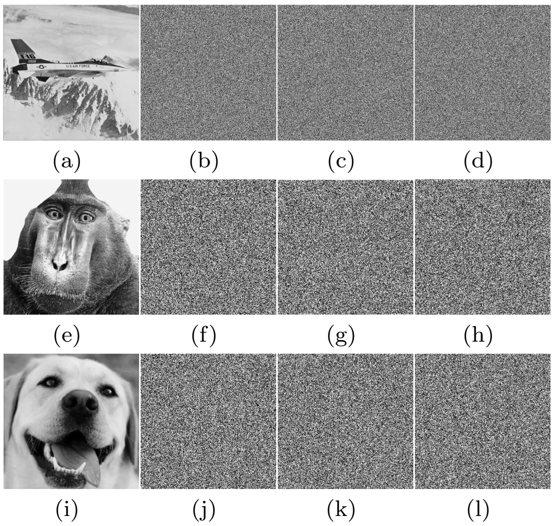

Fig. 16 Image decryption process with the secret key ($x_1(0)$, $x_2(0)$, $x_3(0)$, $x_4(0)$, $z_1(0)$, $z_2(0)$, ρ_1, ρ_2). (a,e,i) Accurate decrypted images with the secret key (1, 1, 1, 1, $\frac{\pi}{2}$, $\frac{\pi}{2}$, 2.6, 0.008). (b,c,d) Inaccurate decrypted images with $\rho_1 = 2.6 + 10^{-14}$, $x_1(0) = 1 + 10^{-14}$, $z_1(0) = \frac{\pi}{2} + 10^{-14}$. (f,g,h) Inaccurate decrypted images with $\rho_2 = 0.008+10^{-14}$, $x_2(0) = 1 + 10^{-14}$, $z_2(0) = \frac{\pi}{2} + 10^{-14}$. (j, k, l) Inaccurate decrypted images with $\rho_1 = 2.6+10^{-14}$, $\rho_2 = 0.008+10^{-14}$, $x_4(0) = 1 + 10^{-14}$.

been found in other neural networks. To demonstrate the usefulness of the proposed AMHNN, we develop an image encryption cryptosystem based on AMHNN. The developed cryptosystem offers numerous advantages over current chaos-based image encryption methods, including a wide key-space, high information entropy, extremely sensitive keys, and good robustness. Hardware experiments using FPGAs are carried out to show the the efficiency of the image cryptosystem.

Acknowledgements This work was partially supported by the National Natural Science Foundation of China(62201204), the Hunan Provincial Natural Science Foundation of China-(2022JJ40514, 2022JJ30624), the Scientific Research Foundation of Hunan Provincial Education Department, China(21B0-345, 21C0200), the Open Fund of Engineering Laboratory of Spatial Information Technology of Highway Geological Disaster Early Warning in Hunan Province, Changsha University of Science and Technology, China(kfj220603), the Open Research Project of the State Key Laboratory of Industrial Control Technology, Zhejiang University,China(No.ICT2023B38).

Data Availability

The data that support the findings of this study are available from the corresponding author, upon reasonable request.

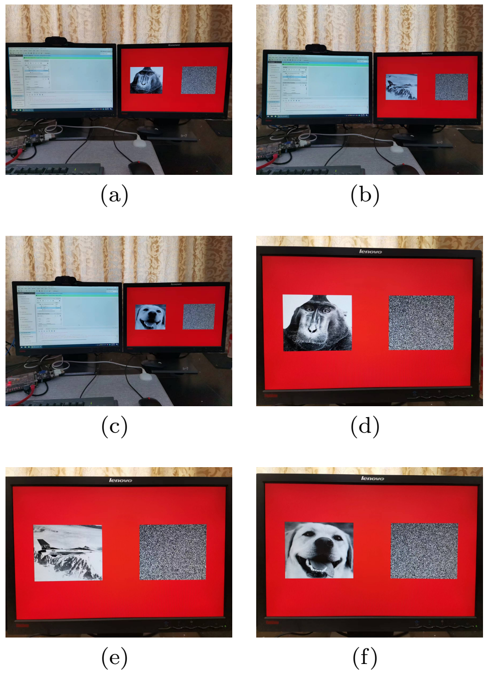

Fig. 17 FPGA-based measurement results. (a-c) FPGA-based experiment environment. (d-f) Original and encrypted images.

Competing Interests

The authors have no relevant financial or non-financial interests to disclose.

Author Contributions

All authors read and approved the final manuscript.

Conflict of interest

The authors declare that they have no conflict of interest.

References

1. Chua, L.: Memristor-the missing circuit element. IEEE Transactions on circuit theory **18**(5), 507–519 (1971)
2. Strukov, D.B., Snider, G.S., Stewart, D.R., Williams, R.S.: The missing memristor found. Nature **453**(7191), 80–83 (2008)
3. Chua, L.: Device modeling via nonlinear circuit elements. IEEE Transactions on Circuits and Systems **27**(11), 1014–1044 (1980)
4. Zhong, H., Li, G., Xu, X.: A generic voltage-controlled discrete memristor model and its application in chaotic map. Chaos, Solitons & Fractals **161**, 112389 (2022)
5. Peng, Y., Sun, K., He, S.: A discrete memristor model and its application in hénon map. Chaos, Solitons & Fractals **137**, 109873 (2020)

6. Lin, H., Wang, C., Hong, Q., Sun, Y.: A multi-stable memristor and its application in a neural network. IEEE Transactions on Circuits and Systems II: Express Briefs **67**(12), 3472–3476 (2020)
7. Xie, W., Wang, C., Lin, H.: A fractional-order multistable locally active memristor and its chaotic system with transient transition, state jump. Nonlinear Dynamics **104**(4), 4523–4541 (2021)
8. Wang, J., Zou, Y., Lei, P., Sherratt, R.S., Wang, L.: Research on recurrent neural network based crack opening prediction of concrete dam. Journal of Internet Technology **21**(4), 1161–1169 (2020)
9. Yu, F., Liu, L., Xiao, L., Li, K., Cai, S.: A robust and fixed-time zeroing neural dynamics for computing time-variant nonlinear equation using a novel nonlinear activation function. Neurocomputing **350**, 108–116 (2019)
10. Yao, W., Yu, F., Zhang, J., Zhou, L.: Asymptotic synchronization of memristive cohen-grossberg neural networks with time-varying delays via event-triggered control scheme. Micromachines **13**(5), 726 (2022)
11. Wang, J., Wu, Y., He, S., Sharma, P.K., Yu, X., Alfarraj, O., Tolba, A.: Lightweight single image super-resolution convolution neural network in portable device. KSII Transactions on Internet & Information Systems **15**(11) (2021)
12. Long, M., Zeng, Y.: Detecting iris liveness with batch normalized convolutional neural network. Computers, Materials & Continua **58**(2), 493–504 (2019)
13. Yao, W., Wang, C., Sun, Y., Zhou, C.: Robust multimode function synchronization of memristive neural networks with parameter perturbations and time-varying delays. IEEE Transactions on Systems, Man, and Cybernetics: Systems **52**(1), 260–274 (2020)
14. Lin, H., Wang, C., Deng, Q., Xu, C., Deng, Z., Zhou, C.: Review on chaotic dynamics of memristive neuron and neural network. Nonlinear Dynamics **106**(1), 959–973 (2021)
15. Yao, Z., Sun, K., He, S.: Firing patterns in a fractional-order fithzhugh–nagumo neuron model. Nonlinear Dynamics **110**(2), 1807–1822 (2022)
16. Yao, W., Wang, C., Sun, Y., Zhou, C., Lin, H.: Exponential multistability of memristive cohen-grossberg neural networks with stochastic parameter perturbations. Applied Mathematics and Computation **386**, 125483 (2020)
17. Xu, L., Qi, G., Ma, J.: Modeling of memristor-based hindmarsh-rose neuron and its dynamical analyses using energy method. Applied Mathematical Modelling **101**, 503–516 (2022)
18. Lin, H., Wang, C., Cui, L., Sun, Y., Xu, C., Yu, F.: Brain-like initial-boosted hyperchaos and application in biomedical image encryption. IEEE Transactions on Industrial Informatics **18**(12), 8839–8850 (2022)
19. Qiu, H., Xu, X., Jiang, Z., Sun, K., Cao, C.: Dynamical behaviors, circuit design, and synchronization of a novel symmetric chaotic system with coexisting attractors. Scientific Reports **13**(1), 1893 (2023)
20. Doubla, I.S., Ramakrishnan, B., Njitacke, Z.T., Kengne, J., Rajagopal, K.: Hidden extreme multistability and its control with selection of a desired attractor in a non-autonomous hopfield neuron. AEU-International Journal of Electronics and Communications **144**, 154059 (2022)
21. Chen, C., Chen, J., Bao, H., Chen, M., Bao, B.: Coexisting multi-stable patterns in memristor synapse-coupled hopfield neural network with two neurons. Nonlinear Dynamics **95**, 3385–3399 (2019)
22. Zhang, S., Zheng, J., Wang, X., Zeng, Z., He, S.: Initial offset boosting coexisting attractors in memristive multi-double-scroll hopfield neural network. Nonlinear Dynamics **102**, 2821–2841 (2020)
23. Lin, H., Wang, C., Sun, J., Zhang, X., Sun, Y., Iu, H.H.: Memristor-coupled asymmetric neural networks: Bionic modeling, chaotic dynamics analysis and encryption application. Chaos, Solitons & Fractals **166**, 112905 (2023)
24. Fahimi, Z., Mahmoodi, M., Nili, H., Polishchuk, V., Strukov, D.: Combinatorial optimization by weight annealing in memristive hopfield networks. Scientific Reports **11**(1), 16383 (2021)
25. Long, M., Peng, F., Li, H.: Separable reversible data hiding and encryption for hevc video. Journal of Real-Time Image Processing **14**, 171–182 (2018)
26. Lai, Q., Lai, C., Zhang, H., Li, C.: Hidden coexisting hyperchaos of new memristive neuron model and its application in image encryption. Chaos, Solitons & Fractals **158**, 112017 (2022)
27. Zhou, S., Wang, X., Zhang, Y., Ge, B., Wang, M., Gao, S.: A novel image encryption cryptosystem based on true random numbers and chaotic systems. Multimedia Systems pp. 1–18 (2022)
28. Chen, Y., Xie, S., Zhang, J.: A hybrid domain image encryption algorithm based on improved henon map. Entropy **24**(2), 287 (2022)
29. Zhou, S., Qiu, Y., Wang, X., Zhang, Y.: Novel image cryptosystem based on new 2d hyperchaotic map and dynamical chaotic s-box. Nonlinear Dynamics **111**(10), 9571–9589 (2023)
30. Bigdeli, N., Farid, Y., Afshar, K.: A robust hybrid method for image encryption based on hopfield neural network. Computers & Electrical Engineering **38**(2), 356–369 (2012)
31. Lai, Q., Wan, Z., Zhang, H., Chen, G.: Design and analysis of multiscroll memristive hopfield neural network with adjustable memductance and application to image encryption. IEEE Transactions on Neural Networks and Learning Systems pp. 1–14 (2022)
32. Yu, F., Shen, H., Yu, Q., Kong, X., Sharma, P.K., Cai, S.: Privacy protection of medical data based on multi-scroll memristive hopfield neural network. IEEE Transactions on Network Science and Engineering p. 726 (2022)
33. Wang, S., Cao, Y., Wen, S., Guo, Z., Huang, T., Chen, Y.: Projective synchroniztion of neural networks via continuous periodic event-based sampling algorithms. IEEE Transactions on Network Science and Engineering **7**(4), 2746–2754 (2020)
34. Yao, W., Wang, C., Sun, Y., Gong, S., Lin, H.: Event-triggered control for robust exponential synchronization of inertial memristive neural networks under parameter disturbance. Neural Networks **164**, 67–80 (2023)
35. Breakspear, M.: Dynamic models of large-scale brain activity. Nature neuroscience **20**(3), 340–352 (2017)
36. Sah, M.P., Yang, C., Kim, H., Muthuswamy, B., Jevtic, J., Chua, L.: A generic model of memristors with parasitic components. IEEE Transactions on Circuits and Systems I: Regular Papers **62**(3), 891–898 (2015)
37. Chua, L.: If it's pinched it's a memristor. Semiconductor Science and Technology **29**(10), 104001 (2014)
38. Chua, L.: Everything you wish to know about memristors but are afraid to ask. Radioengineering **24**, 319–368 (2015)
39. Jiang, Y., Li, C., Zhang, C., Zhao, Y., Zang, H.: A double-memristor hyperchaotic oscillator with complete amplitude control. IEEE Transactions on Circuits and Systems I: Regular Papers **68**(12), 4935–4944 (2021)
40. Bao, H., Hua, Z., Li, H., Chen, M., Bao, B.: Memristor-based hyperchaotic maps and application in auxiliary

classifier generative adversarial nets. IEEE Transactions on Industrial Informatics **18**(8), 5297–5306 (2022)
41. Ping, J., Zhu, S., Shi, M., Wu, S., Shen, M., Liu, X., Wen, S.: Event-triggered finite-time synchronization control for quaternion-valued memristive neural networks by an non-decomposition method. IEEE Transactions on Network Science and Engineering pp. 1–10 (2023)
42. Ye, X., Wang, X.: Hidden oscillation and chaotic sea in a novel 3d chaotic system with exponential function. Nonlinear Dynamics pp. 1–10 (2023)
43. Wen, S., Zeng, Z., Huang, T., Meng, Q., Yao, W.: Lag synchronization of switched neural networks via neural activation function and applications in image encryption. IEEE Transactions on Neural Networks and Learning Systems **26**(7), 1493–1502 (2015)
44. Liu, L., Zhang, L., Jiang, D., Guan, Y., Zhang, Z.: A simultaneous scrambling and diffusion color image encryption algorithm based on hopfield chaotic neural network. IEEE Access **7**, 185796–185810 (2019)
45. Zhou, S., Wang, X., Zhang, Y.: Novel image encryption scheme based on chaotic signals with finite-precision error. Information Sciences **621**, 782–798 (2023)
46. Xia, Z., Wang, L., Tang, J., Xiong, N.N., Weng, J.: A privacy-preserving image retrieval scheme using secure local binary pattern in cloud computing. IEEE Transactions on Network Science and Engineering **8**(1), 318–330 (2021)
47. Benkouider, K., Vaidyanathan, S., Sambas, A., Tlelo-Cuautle, E., Abd El-Latif, A.A., Abd-El-Atty, B., Bermudez-Marquez, C.F., Sulaiman, I.M., Awwal, A.M., Kumam, P.: A new 5-d multistable hyperchaotic system with three positive lyapunov exponents: Bifurcation analysis, circuit design, fpga realization and image encryption. IEEE Access **10**, 90111–90132 (2022)
48. Yao, W., Gao, K., Zhang, Z., Cui, L., Zhang, J.: An image encryption algorithm based on a 3d chaotic hopfield neural network and random row–column permutation. Frontiers in Physics **11**, 1162887 (2023)
49. Jithin, K., Sankar, S.: Colour image encryption algorithm combining arnold map, dna sequence operation, and a mandelbrot set. Journal of Information Security and Applications **50**, 102428 (2020)
50. Wu, Y., Noonan, J.P., Agaian, S., et al.: Npcr and uaci randomness tests for image encryption. Cyber journals: multidisciplinary journals in science and technology, Journal of Selected Areas in Telecommunications (JSAT) **1**(2), 31–38 (2011)
51. Ye, X., Wang, X., Gao, S., Mou, J., Wang, Z., Yang, F.: A new chaotic circuit with multiple memristors and its application in image encryption. Nonlinear Dynamics **99**, 1489–1506 (2020)
52. Xu, C., Sun, J., Wang, C.: An image encryption algorithm based on random walk and hyperchaotic systems. International Journal of Bifurcation and Chaos **30**(04), 2050060 (2020)
53. Lai, Q., Wan, Z., Zhang, H., Chen, G.: Design and analysis of multiscroll memristive hopfield neural network with adjustable memductance and application to image encryption. IEEE Transactions on Neural Networks and Learning Systems pp. 1–14 (2022)
54. Wang, T., Song, L., Wang, M., Zhuang, Z.: A novel image encryption algorithm based on parameter-control scroll chaotic attractors. IEEE Access **8**, 36281–36292 (2020)
55. Lin, H., Wang, C., Yu, F., Xu, C., Hong, Q., Yao, W., Sun, Y.: An extremely simple multiwing chaotic system: dynamics analysis, encryption application, and hardware implementation. IEEE Transactions on Industrial Electronics **68**(12), 12708–12719 (2020)
56. Sambas, A., Vaidyanathan, S., Tlelo-Cuautle, E., Abd-El-Atty, et al.: A 3-d multi-stable system with a peanut-shaped equilibrium curve: Circuit design, fpga realization, and an application to image encryption. IEEE Access **8**, 137116–137132 (2020)
57. Slavova, A., Tetzlaff, R.: Edge of chaos in memristor cnn with hysteresis and applications in pattern formation. 2021 IEEE International Symposium on Circuits and Systems (ISCAS) pp. 1–4 (2021)
58. Kong, X., Yu, F., Yao, W., Xu, C., Zhang, J., Cai, S., Wang, C.: A class of 2n+1 dimensional simplest hamiltonian conservative chaotic systems and fast image encryption schemes. Applied Mathematical Modelling (2023). DOI 10.1016/j.apm.2023.10.004